Journal of Power Sources 189 (2009) 814–817

Contents lists available at ScienceDirect

Journal of Power Sources

journal homepage: www.elsevier.com/locate/jpowsour

Short communication

^{119}Sn Mössbauer parameters as predictive tool for future Sn-based negative electrode materials

S. Naille, J.-C. Jumas, P.-E. Lippens, J. Olivier-Fourcade*

ICG/AIME (UMR 5253 CNRS), Université Montpellier II, CC1502, Place E. Bataillon, 34095 Montpellier cedex 5, France

ARTICLE INFO

Article history:
Received 26 June 2008
Accepted 21 July 2008
Available online 30 July 2008

Keywords:
Sn-based electrode materials
Predictive model
Electronic density
^{119}Sn Mössbauer hyperfine parameters

ABSTRACT

Thanks to the ^{119}Sn Mössbauer hyperfine parameters, it is possible to analyze and predict Li reaction mechanisms with Sn-based negative electrodes for Li-ion batteries. The present approach is based on the interpretation of the ^{119}Sn Mössbauer hyperfine parameters: isomer shift (δ) and quadrupole splitting (Δ) by considering: (i) the analysis of the ^{119}Sn Mössbauer hyperfine parameters of the Li–Sn alloys used as model compounds, (ii) their interpretation from some physicochemical parameters (Li/Sn ratio, crystal structure, electronic density as defined by Hume-Rothery), and (iii) the proposition of an experimental based model to understand Li lithiation/delithiation mechanisms and predict electrochemical performances for Sn-based compounds including the effects of volume variations, particle coalescence or SEI formation.

1. Introduction

The improvement of Li-ion battery performances needs the search of new electrode materials and a better understanding of their electrochemical mechanisms. Among the various possible new negative electrode materials, Sn-based materials are very promising [1–4]. Indeed, the possible formation with Sn of Li-rich alloys as Li_7Sn_2 or $Li_{22}Sn_5$ allows obtaining high storage capacities (up to 990 mAh g^{-1}). Unfortunately, the Li–Sn alloying leads to high volume variations of the particles on cycling and therefore strongly limits the reversibility. In order to solve this problem, many approaches have been analyzed in a recent paper [5]. Among the different possibilities, the use of composite materials [6,7] or multi-element metallic materials [8–10] seems to be the most favorable. The interest in these materials has risen since the commercialization by Sony Company of the newly developed Sn-based (Co–Sn–C) negative electrode [11] with improved cycleability.

For Sn-based materials, ^{119}Sn Mössbauer spectroscopy, the recoil-free resonant absorption of γ-rays, is really suitable to study the various steps of a synthesis or a charge/discharge process of electrode materials, *in situ* by using specific test cells or *ex situ* by extracting the material from the cell at a given point of the charge/discharge curve [12]. The technique allows therefore the study of nanostructured materials. Mössbauer spectroscopy is further helpful because it can give information not only on static properties (such as crystal structure, magnetic properties, valence state and bonding) but also on dynamic properties (such as diffusion, mechanic vibrations of nanoparticles, super paramagnetic relaxation, electron hopping, etc.). For ^{119}Sn, two main hyperfine interactions can be distinguished: (i) electric monopole interaction, detectable as a line shift (isomer shift, δ) and (ii) electric quadrupole interaction, detectable as a line splitting (quadrupole splitting, Δ). The hyperfine parameters, δ and Δ, respectively proportional to the *s* electronic density at the nucleus and to the main component of the electric field gradient, allow characterizing the Sn oxidation state and coordination.

The aim of this paper is to propose an experimental model used to analyze the reaction mechanisms during different steps of Sn-based materials lithiation/delithiation and to predict their electrochemical performances as possible negative electrodes and different processes that can occur as the volume expansion, the particles coalescence or the SEI formation. The knowledge of the hyperfine parameters (δ and Δ) of the different Li–Sn crystalline phases (Li_2Sn_5, LiSn, Li_7Sn_3, Li_5Sn_2, $Li_{13}Sn_5$, Li_7Sn_2 and $Li_{22}Sn_5$) obtained by ball-milling [13] is very appropriate to analyze the data obtained for these Sn-based materials in terms of some physicochemical properties (lithium content, crystal structure or electronic density). By answering to three main questions: (i) "what is the Li_xSn composition during lithiation/delithiation of Sn-based materials?" (ii) "what is the network nature in these Li_xSn alloys?" and (iii) "is it possible to predict the electrochemical performances of new Sn-based materials?", we will show that ^{119}Sn Mössbauer spectroscopy can be used as a powerful predictive technique in the field of Li-ion batteries.

* Corresponding author. Tel.: +33 4 67143346; fax: +33 4 67143304.
E-mail address: jolivier@univ-montp2.fr (J. Olivier-Fourcade).

0378-7753/$ – see front matter © 2008 Elsevier B.V. All rights reserved.
doi:10.1016/j.jpowsour.2008.07.058

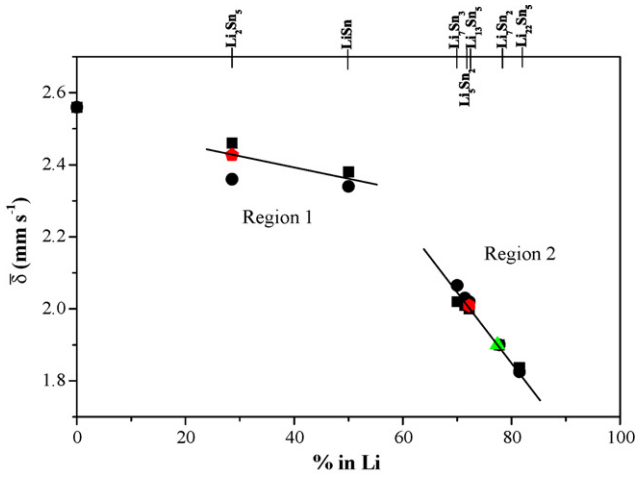

Fig. 1. $\bar{\delta}$–%Li correlation diagram for the Li–Sn alloys ((■) [12] and (●) [13]) and for products obtained from the lithiation of Sn-0.4BPO_4 ((⬟) and (⬢) [14]) and Ni_3Sn_4 ((▲) [10]).

2. What is the Li_xSn composition?

Fig. 1 shows the variations of the isomer shift mean value ($\bar{\delta}$) as a function of the Li content. The $\bar{\delta}$ values are calculated for the different Li–Sn alloys taking into account the proportion of each site in accordance with the crystal structure [13,14].

By using this $\bar{\delta}$–%Li correlation diagram, it is therefore possible to know the proportion of lithium allied with tin at any point of an electrochemical cycle. Indeed, the value of $\bar{\delta}$ will determine the percentage of lithium constituting the alloy formed and therefore it is possible to deduct the proportion of lithium that is not involved in the electrochemical mechanism. In the case of Sn-0.4BPO_4 (Fig. 2), the different Li–Sn alloys are formed during the first discharge [15]. However, the Li content in the Li_xSn alloy formed at 1.2 Li is only $x = 0.4$ if we consider $\bar{\delta}$ (Fig. 1), which explains that a certain amount of lithium is necessary at the beginning of the first discharge to form a SEI and to reduce the interfacial Sn^{II} component obtained during the synthesis of such composite [16]. Further in the discharge,

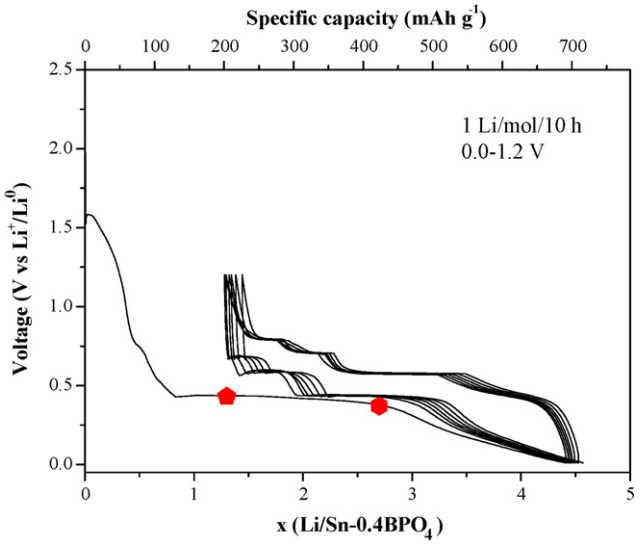

Fig. 2. Voltage profile of Sn-0.4BPO_4 electrode. (⬟) and (⬢) are the electrode compositions characterized by ^{119}Sn Mössbauer spectroscopy for the determination of the type and the composition of the Li–Sn alloys electrochemically formed.

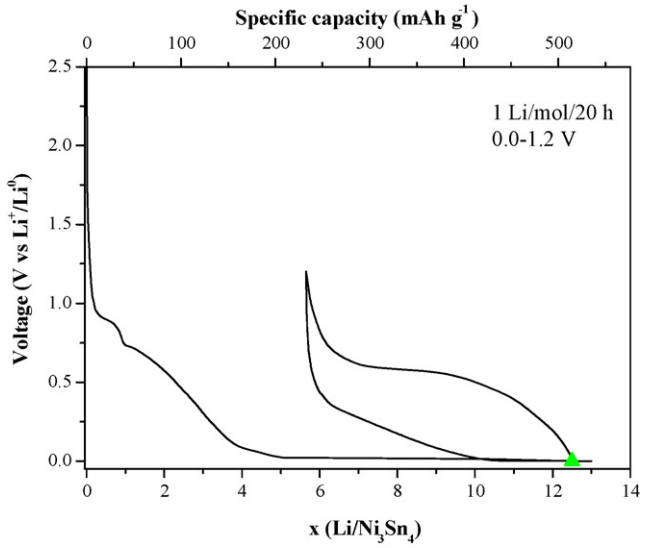

Fig. 3. Voltage profile of Ni_3Sn_4 electrode. (▲) is the electrode composition characterized by ^{119}Sn Mössbauer spectroscopy for the determination of the type and the composition the Li–Sn alloy electrochemically formed.

the value of x reached 2.6 in Li_xSn (Figs. 1 and 2) and the Li_7Sn_2 composition is obtained at the end of the first discharge.

With Sn-based intermetallics compounds, lithium reacts directly to form a Li-rich Li_xSn alloy. For instance, with Ni_3Sn_4 of which the electrochemical curve is given in Fig. 3, this is the Li_7Sn_2 alloy which is formed on the biphasic plateau (Fig. 1). The first part of the discharge is mainly due to the formation of a stable SEI and consumes four Li [17]. This kind of mechanism is observed for most of the Sn-rich intermetallics (e.g. $FeSn_2$ [18], $CoSn_2$ [19], $MnSn_2$ [20], $NbSn_2$ [21]) except for Cu_6Sn_5 for which a ternary phase Li_2CuSn is firstly formed [22].

3. What is the Li_xSn network nature?

The Fig. 4 has been obtained by plotting the (δ, Δ) points of the different Li–Sn alloys obtained by ball-milling [13]. From this Δ–δ correlation diagram, it is rather easy to identify two main regions that are characteristic of material families with given structural and electronic properties. The first region is the domain of Sn-rich alloys with continuous networks based on Sn—Sn bonds that provide a strong "covalo-metallic" character. The Sn local structures are octahedral (more or less distorted) and Sn is surrounded only by either six Sn (1a) or by four Sn and two Li (1b) atoms. The second region is the domain of Li-rich alloys with lattices based on Li^+ close packing that gives an "iono-metallic" character. The Sn local structure in this case is cubic and the Sn-network is uncontinuous. There are three types of environments with Sn surrounded by either six Li and two Sn (2a) or seven Li and one Sn (2b) or eight Li (2c) atoms.

This diagram allows identifying the nature and composition of the Li–Sn alloys formed during cycling. The formation of the different alloys during the first discharge is confirmed for Sn-0.4BPO_4. Indeed, Li_2Sn_5 is formed at the early stage of the process whereas $Li_{13}Sn_5$ is formed later (Fig. 4). The nature and the composition of the single alloy formed by the lithiation of a Sn-based intermetallic compound (e.g. Ni_3Sn_4) is Li_7Sn_2 rather than $Li_{22}Sn_5$ as often mentioned in the literature (Fig. 4). The formation of this alloy leads to a decrease of 20% of the theoretical capacity in term of electrochemical performances.

The Δ–δ correlation diagram also indicates the type of bonds (covalent, ionic, metallic), the type of lattice and the different tin

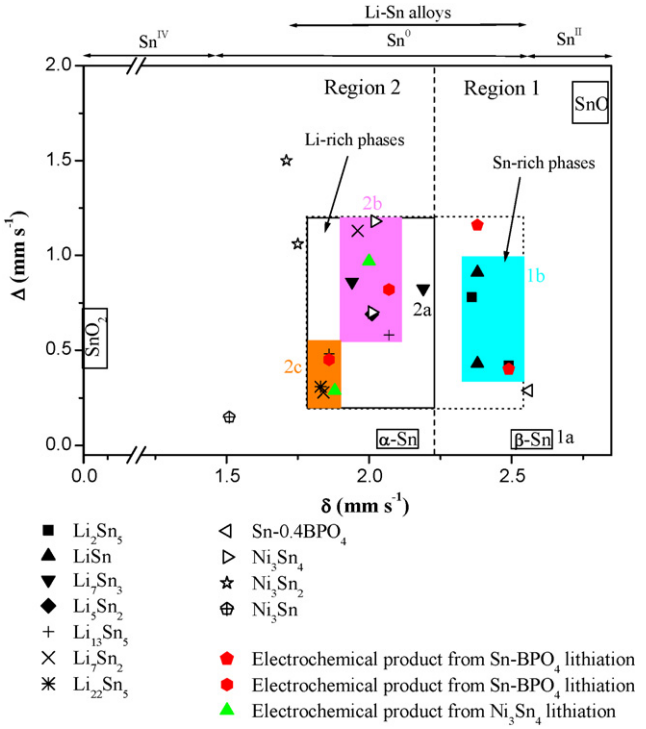

Fig. 4. Δ–δ correlation diagram for the different tin sites of the Li–Sn alloys, for some Sn-based intermetallics and composites and some of their electrochemical products.

crystallographic sites for Sn-based materials by considering their Mössbauer parameters. The knowledge of the Mössbauer hyperfine parameters (δ and Δ) for Sn-based materials (Table 1) can thus be useful in order to predict the reaction mechanisms and therefore the electrochemical performances.

For $\delta < 1.8$ mm s^{-1}, there is no electrochemical reaction between lithium and Sn-based intermetallic compounds. These δ values are obtained for Sn-based intermetallics rich in transition metal. Fig. 4 shows that Ni_3Sn and Ni_3Sn_2 have lower δ than the Li-richest Li_xSn alloys. They are considered as electrochemically inactive, as their specific capacities never exceed 60 mAh g^{-1} [23]. This is confirmed for Mn–Sn [20], Fe–Sn [24] and Co–Sn [25] systems. When 1.8 mm s^{-1} < δ < 2.3 mm s^{-1}, the electrochemical reaction between lithium and Sn-based intermetallics involves weak structural modifications of the Sn-network thanks to the direct formation of Li-rich Li_xSn alloys as for Ni_3Sn_4 (Fig. 4). With these intermetallics, moderate capacities can be reached (~400 mAh g^{-1}) but good cycling performances are obtained as the transition metal, which acts as a "buffer", can also minimize the volume expansion during the alloying process [11,17–22]. With $\delta > 2.3$ mm s^{-1}, electrochemical reaction with lithium engages strong volume variations due to strong structural modifications of the Sn-network with the formation of Sn-rich Li–Sn alloys followed by Li-rich alloys. In this case, high capacities are obtained but the cycling performances are very poor. Therefore, the dispersion of the tin element in oxide inactive matrices (BPO_4, $CaSiO_3$, Al_2O_3 and so on), which absorb the volume expansion, can improve the electrochemical performances (over 500 mAh g^{-1}) [7,16,26,27].

4. Is it possible to predict the electrochemical performances of new Sn-based materials?

The Hume-Rothery electronic density [e_{av}] is an empirically defined quantity that can be used to study the amount of electrons involved in bonds and can only be used for atoms without partially filled shields (d, f) [28]. For a A—B bond, the relation is given by:

$$[e_{av}] = \frac{N(A) \times n_v(A) - N(B) \times n_v(B)}{N(A) + N(B)} \quad (1)$$

where N(A) and N(B) are the number of atoms A and B respectively in the molecular unit and n_v(A) and n_v(B) are the number of valence electrons for atoms A and B respectively. For the Li–Sn system, one considers that all the valence electrons are involved in bonds (one electron for lithium and four electrons for tin). The $\bar{\delta}$–[e_{av}] correlation diagram is shown for the Li–Sn alloys in Fig. 5 and the two regions discussed above can be distinguished depending on the slope of the correlation lines. The region 1, with high electronic density ([e_{av}] > 2.4), corresponds to the Sn-based lattices whereas the region 2, with low electronic density (1.5 < [e_{av}] < 2.4), corresponds to the Li-based lattices.

It is therefore possible to determine [e_{av}] for any Sn-based material by considering its $\bar{\delta}$ (Fig. 5) and to analyze the reaction mechanisms. In region 1, for [e_{av}] > 2.4, $\bar{\delta}$ is almost constant but [e_{av}] is related to the lattice dimensionality which depends on the tin coordination. A decrease of $\bar{\delta}$ corresponds to an increase of the covalent character of the bonds which leads to strong dimensional modifications of the Sn-network. We have already seen that tin needs therefore to be dispersed in an inactive matrix in this region as for example Sn-0.4BPO_4. In the region 2, for 1.5 < [e_{av}] < 2.4 (e.g. Ni_3Sn_4), $\bar{\delta}$ varies as a function of the Sn-cluster dimensionality but variations of [e_{av}] are small between the intermetallic and the electrochemically formed Li–Sn alloy, and thus the Sn-network will not suffer only minor volume variations. For [e_{av}] < 1.5, there is no

Table 1
Hyperfine parameters of Sn-0.4BPO_4, Ni_3Sn, Ni_3Sn_2, Ni_3Sn_4 and $CoSn_2$: the different types of tin sites used in the Mössbauer fitting procedure and their relative intensity (I), the values of the isomer shift (δ), the mean isomer shift ($\bar{\delta}$), and the quadrupole splitting (Δ). The average electronic densities [e_{av}] of these Sn-based materials, deduced from the $\bar{\delta}$–[e_{av}] correlation diagram (Fig. 5), are also given

Sn-based materials	Tin sites	I (%)	δ (mm s^{-1})	$\bar{\delta}$ (mm s^{-1})	Δ (mm s^{-1})	[e_{av}]
Sn-0.4BPO_4	4a	100	2.56 (3)[a]	2.56	0.29 (3)[a]	4
Ni_3Sn	2c	100	1.50 (3)[b]	1.50	0.15 (3)[b]	0.98
	4c	50	1.75 (3)[b]		1.03 (3)[b]	
Ni_3Sn_2	4c	50	1.73 (3)[b]	1.74	1.50 (3)[b]	1.38
	4i	50	2.01 (4)[b,c]		0.78 (6)[b,c]	
Ni_3Sn_4	4i	50	2.02 (4)[b,c]	2.01	1.18 (6)[b,c]	1.86
$CoSn_2$	8h	100	2.14 (3)[c]	2.14	0.77 (3)[c]	2.09

[a] See Ref. [16].
[b] See Ref. [23].
[c] See Ref. [10].

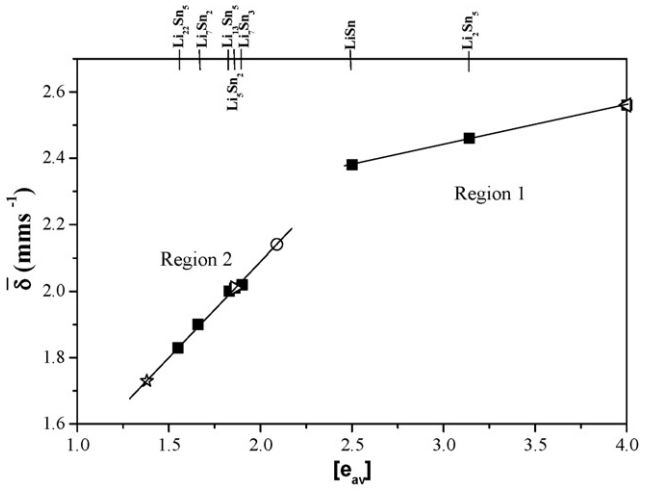

Fig. 5. $\bar{\delta}$–[e_{av}] correlation diagram for the Li–Sn alloys. [e_{av}] of Sn-BPO_4 (◁), Ni_3Sn_4 (▷), Ni_3Sn_2 (☆) and $CoSn_2$ (◯) are determined by plotting their $\bar{\delta}$ on the correlation lines.

formation of Li–Sn alloys with the Sn-poor intermetallics, as for Ni_3Sn_2.

Furthermore, the $\bar{\delta}$–[e_{av}] correlation diagram allows determining the electronic average population per transition metal (M), n_v(M) with M = A and taking into account n_v(B) = n_v(Sn) = 4 in (1), by considering $\bar{\delta}$. If n_v(M) < 1, the formation of the electrochemical product Li_xSn is rather difficult (e.g. for Sn-based intermetallics located in region 2) if not possible (e.g. for Sn-based intermetallics located below region 2) due to the important formation of a solid electrolyte interphase (SEI) related to the accumulation of negative charges at the electrode/electrolyte interface. The Li atoms are not able to provide electrons to Sn atoms in order to form Li–Sn alloys without any lattice modifications, Sn atoms being donor electrons. Moreover, the SEI thickness is proportional to the gap to 1. Indeed, n_v(Ni) for Ni_3Sn_4 has a lower value than n_v(Co) in $CoSn_2$ and the SEI layer is more important for Ni_3Sn_4 than for $CoSn_2$ [10]. This means that the lower the n_v(M) value, the larger the SEI thickness.

5. Conclusion

Experimental determination of the Mössbauer parameters for Sn-based negative electrodes allows analyzing reaction mechanisms leading to the formation of Li–Sn alloys during the electrochemical cycling. A model has been proposed based on the analysis of three correlation diagrams: $\bar{\delta}$–%Li, Δ–δ and $\bar{\delta}$–[e_{av}], that allows identifying and understanding the electrochemical mechanisms from Mössbauer parameters measured either *ex situ* or *in situ* during lithiation/delithiation. The determination of the Li–Sn alloys formed during cycling, including composition, structure and type of lattice can be done from the $\bar{\delta}$–%Li and Δ–δ correlation diagrams. It is also possible to predict the electrochemical performances of a possible Sn-based negative electrode as a Sn-based material react with lithium when $\bar{\delta} > 1.8\,mm\,s^{-1}$ ([e_{av}] > 1.5). The capacity ranges can be known from the type of the Li–Sn alloys that can be formed with the Δ–δ correlation diagram. A 20 % decrease of the specific capacity should be expected in the case of Li_7Sn_2 formation rather than $Li_{22}Sn_5$. The cycling retention due to the effect of volume variations can be predicted from the main features of the materials from the Δ–δ and $\bar{\delta}$–[e_{av}] correlation diagrams. Finally, the importance of the SEI layer can also be pointed out, especially the thickness which is proportional to the decrease of n_v(M). This number can be obtained from [e_{av}] by considering the $\bar{\delta}$–[e_{av}] correlation diagram.

Acknowledgements

This work has been carried out in the framework of ALISTORE network of Excellence (SES6-CT-2003-503532) and Mössbauer platform. The authors are grateful to the European Community and to the Région Languedoc Roussillon (France) for their financial support.

References

[1] I.A. Courtney, J.R. Dahn, J. Electrochem. Soc. 144 (1997) 2045.
[2] A.H. Whitehead, J.M. Elliott, J.R. Owen, J. Power Sources 81 (1999) 33.
[3] A.S. Yu, R. Frech, J. Power Sources 104 (2002) 97.
[4] Y.N. Nuli, S.L. Zhao, Q.Z. Qin, J. Power Sources 114 (2003) 113.
[5] D. Larcher, S. Beattie, M. Morcrette, K. Edström, J.-C. Jumas, J.-M. Tarascon, J. Mater. Chem. 17 (2007) 3759.
[6] L.Y. Beaulieu, D. Larcher, R.A. Dunlap, J.R. Dahn, J. Alloys Compd. 297 (2000) 122.
[7] A. Aboulaich, M. Mouyane, F. Robert, P.-E. Lippens, J. Olivier-Fourcade, P. Willmann, J.-C. Jumas, J. Power Sources 174 (2007) 1224.
[8] O. Mao, R.L. Turner, I.A. Courtney, B.D. Fredericksen, M.I. Buckett, L.J. Krause, J.R. Dahn, Electrochem, Solid State Lett. 2 (1999) 3.
[9] S. Sharma, L. Fransson, E. Sjöstedt, L. Nordström, B. Johansson, K. Edström, J. Electrochem. Soc. 150 (2003) A330.
[10] S. Naille, C.M. Ionica-Bousquet, F. Robert, F. Morato, P.-E. Lippens, J. Olivier-Fourcade, J. Power Sources 174 (2007) 1091.
[11] H. Tanizaki, A. Omaru, US Patent 0,053,131 A1 (2004).
[12] F. Robert, P.-E. Lippens, J. Olivier-Foucade, J.-C. Jumas, M. Morcrette, J. Power Sources 146 (2005) 492.
[13] F. Robert, P.-E. Lippens, J. Olivier-Fourcade, J.-C. Jumas, F. Gillot, M. Morcrette, J.-M. Tarascon, J. Solid State Chem. 180 (2007) 339.
[14] R.A. Dunlap, D.A. Small, D.D. MacNeil, M.N. Obravac, J.R. Dahn, J. Alloys Compd. 289 (1999) 135.
[15] A. Aboulaich, Ph.D. thesis, Université Montpellier II, France, December 2007.
[16] A. Aboulaich, F. Robert, P.-E. Lippens, L. Aldon, J. Olivier-Fourcade, P. Willmann, J.-C. Jumas, Hyperfine Interact. 167 (2006) 733.
[17] K.K.D. Ehinon, S. Naille, R. Dedryvère, P.-E. Lippens, J.-C. Jumas, D. Gonbeau, Chem. Mater. 20 (2008) 5388.
[18] O. Mao, R.A. Dunlap, I.A. Courtney, J.R. Dahn, J. Electrochem. Soc. 145 (1998) 4195.
[19] C.M. Ionica-Bousquet, P.-E. Lippens, L. Aldon, J. Olivier-Fourcade, J.-C. Jumas, Chem. Mater. 18 (2006) 6442.
[20] L.Y. Beaulieu, J.R. Dahn, J. Electrochem. Soc. 147 (2000) 3237.
[21] S. Naille, M. Mouyane, M. El Amraoui, P.-E. Lippens, J.-C. Jumas, J. Olivier-Fourcade, Hyperfine Interact., in press.
[22] W. Choi, J.Y. Lee, H.S. Lim, Electrochem. Commun. 6 (2004) 816.
[23] S. Naille, P.-E. Lippens, F. Morato, J. Olivier-Fourcade, Hyperfine Interact. 167 (2006) 785.
[24] O. Mao, J.R. Dahn, J. Electrochem. Soc. 146 (1999) 414.
[25] C.M. Ionica, Ph.D. thesis, Université Montpellier II, France, November 2005.
[26] M. Mouyane, P.-E. Lippens, M. Womes, B. Ducourant, J. Olivier-Fourcade, J.-C. Jumas, Hyperfine Interact., in press.
[27] J.-H. Ahn, G.X. Wang, J. Yao, H.K. Liu, S.X. Dou, J. Power Sources 119–121 (2003) 45.
[28] W. Hume-Rothery, H.M. Powell, Z. Kristallogr. 91 (1935) 23.